International Journal of Impact Engineering 71 (2014) 17–33

Contents lists available at ScienceDirect

International Journal of Impact Engineering

journal homepage: www.elsevier.com/locate/ijimpeng

Review

# Assessing punching shear failure in reinforced concrete flat slabs subjected to localised impact loading

K. Micallef [a], J. Sagaseta [a,*], M. Fernández Ruiz [b], A. Muttoni [b]

[a] Department of Civil and Environmental Engineering, University of Surrey, Guildford GU2 7XH, UK
[b] IS-BETON, École Polytechnique Fédérale de Lausanne (ÉPFL), Lausanne CH-1015, Switzerland

ARTICLE INFO

*Article history:*
Received 2 September 2013
Received in revised form
27 February 2014
Accepted 6 April 2014
Available online 19 April 2014

*Keywords:*
Punching shear
Flat slabs
Impact loading
Strain-rate effects
Critical shear crack theory

ABSTRACT

Reinforced concrete flat slab structures are used widely in construction projects due to their economic and functional advantages. Punching shear failure in such structures can have catastrophic effects in the case of, for example, multi-storey framed structures and the designer aims to ensure that ductile flexural deformation occurs before the brittle shear failure.

Shear mechanisms generally govern the behaviour of reinforced concrete structures subjected to localised impact loads. Existing experimental results investigating punching shear in flat slabs subjected to impact loading shows that when increasing the loading rate, the punching shear strength also increases whereas the deformation capacity reduces. This behaviour is due to a combination of inertial effects and material strain-rate effects which leads to a stiffer behaviour of the slab for higher loading rates. This can also lead to a change of mode of failure from flexural to pure punching shear with increasing loading rates. Current empirical formulae for punching shear are unable to predict this behaviour since the slab deformations are not considered for calculating the punching shear strength.

This paper presents an analytical model based on the Critical Shear Crack Theory which can be applied to flat slabs subjected to impact loading. This model is particularly useful for cases such as progressive collapse analysis and flat slab-column connections subjected to an impulsive axial load in the column. The novelty of the approach is that it considers (a) the dynamic punching shear capacity and (b) the dynamic shear demand, both in terms of the slab deformation (slab rotation). The model considers inertial effects and material strain-rate effects although it is shown that the former has a more significant effect. Moreover, the model allows a further physical understanding of the phenomena and it can be applied to different cases (slabs with and without transverse reinforcement) showing a good correlation with experimental data.



## 1. Introduction

### 1.1. High-rate loading

The design of most reinforced concrete (RC) structures is typically governed by ultimate limit state performance of the various structural elements when subjected to static loading, e.g. dead (or permanent) loads and live (or imposed or variable) loads. Whilst the former are typically static in nature (e.g. structure's self-weight, finishes etc.), the magnitude of live loading tends to be variable with time (e.g. pedestrian or vehicular traffic loading). However, in most cases, such loadings can be idealised as quasi-static, since the rate at which this loading is applied, typically described by the strain-rate, $\dot{\varepsilon}$, is of a very small magnitude.

Fig. 1 gives typical ranges of strain-rates for different loading sources.

Dynamic loads are often also idealised as being quasi-static or replaced by equivalent static loadings but in the case of extreme events, such as blast or impact loading, such simplifications could be inadequate and further consideration is necessary [2]. Reliable structural modelling is essential to accurately predict the response and damage in structures subjected to loads at high strain-rates. The effects of strain-rate effects can be considered on two levels, viz. the effects on the material properties of the structure's constituents and the effects on the response of the structure itself.

### 1.2. Effect of strain-rate on material properties

The effect of strain-rate on the mechanical properties of most engineering materials is well-known. This includes the

* Corresponding author. Tel.: +44 (0) 1483 686649; fax: +44 (0) 1483 682135.
*E-mail address:* j.sagaseta@surrey.ac.uk (J. Sagaseta).

http://dx.doi.org/10.1016/j.ijimpeng.2014.04.003
0734-743X/

**Nomenclature**

*Latin lower case*

| | |
|---|---|
| $a$ | penetration constant, [$T^{-2}$] |
| $b$ | penetration constant, [$L^{-2}$] |
| $b_0$ | punching control perimeter, [L] |
| $c_1$ | tension softening constant, [−] |
| $c_2$ | tension softening constant, [−] |
| $c_{s0}$ | slab initial damping co-efficient, [M $T^{-1}$] |
| $c_s$ | slab damping co-efficient, [M $T^{-1}$] |
| $d_g$ | concrete maximum aggregate size, [L] |
| $d_{g0}$ | reference concrete aggregate size, [L] |
| $d_v$ | shear-resisting slab effective depth, [L] |
| $d$ | slab effective depth, [L] |
| $f_c$ | concrete compressive strength, [M $L^{-1}$ $T^{-2}$] |
| $f_{c0}$ | reference concrete compressive strength, [M $L^{-1}$ $T^{-2}$] |
| $f_{ct}$ | concrete tensile strength, [M $L^{-1}$ $T^{-2}$] |
| $f_y$ | steel reinforcement yield stress, [M $L^{-1}$ $T^{-2}$] |
| $g$ | acceleration due to gravity, [L $T^{-2}$] |
| $h_i$ | drop height of impactor, [L] |
| $h_s$ | slab thickness, [L] |
| $k_c$ | contact stiffness, [M $T^{-2}$] |
| $k_{s0}$ | slab initial stiffness, [M $T^{-2}$] |
| $k_s$ | slab stiffness, [M $T^{-2}$] |
| $m_i$ | mass of impactor, [M] |
| $m_{s0}$ | slab initial mass, [M] |
| $m_s$ | slab mass, [M] |
| $r_c$ | column radius, [L] |
| $r_s$ | position of zero bending moment with respect to support axis, [L] |
| $r_{s0}$ | initial position of zero bending moment during contact time, [L] |
| $t$ | time, [T] |
| $t_c$ | contact time, [T] |
| $t_E$ | time to peak response, [T] |
| $u_i(t)$ | impactor displacement, [L] |
| $\dot{u}_i(t)$ | impactor velocity, [L $T^{-1}$] |
| $\ddot{u}_i(t)$ | impactor acceleration, [L $T^{-2}$] |
| $u_s(t)$ | slab displacement, [L] |
| $\dot{u}_s(t)$ | slab velocity, [L $T^{-1}$] |
| $\ddot{u}_s(t)$ | slab acceleration, [L $T^{-2}$] |
| $v_c$ | concrete shear wave velocity, [L $T^{-1}$] |
| $w$ | crack width, [L] |
| $w_c$ | maximum crack width, [L] |

*Latin upper case*

| | |
|---|---|
| $\overline{A}_x$ | projected contact areas in the $X$ direction for an unit crack area, [−] |
| $\overline{A}_y$ | projected contact areas in the $Y$ direction for an unit crack area, [−] |
| $A$ | impactor section pressure, [M $L^{-1}$ $T^{-2}$] |
| $E_c$ | concrete elastic modulus, [M $L^{-1}$ $T^{-2}$] |
| $E_s$ | steel reinforcement elastic modulus, [M $L^{-1}$ $T^{-2}$] |
| $G_c$ | concrete shear modulus, [M $L^{-1}$ $T^{-2}$] |
| $G_F$ | fracture energy, [M $T^{-2}$] |
| $G_{F0}$ | reference fracture energy, [M $T^{-2}$] |
| $K$ | material constant, [$M^{-1}$ $L^2$ $T^2$] |
| $L_{eff}$ | slab effective span, [L] |
| $M_{Rd}$ | unit slab flexural capacity, [M L $T^{-2}$] |
| $M_{sd}$ | unit slab bending moment, [M L $T^{-2}$] |
| $N$ | crack normal force component, [M L $T^{-2}$] |
| $P(t)$ | contact force, [M L $T^{-2}$] |
| $\dot{P}$ | loading rate, [M L $T^{-3}$] |
| $P'$ | section limiting load, [M L $T^{-2}$] |
| $R_i$ | impactor radius, [L] |
| $S$ | crack shear force component, [M L $T^{-2}$] |
| $V$ | penetration velocity, [L $T^{-1}$] |
| $V'$ | velocity factor, [−] |
| $V_0$ | impactor initial velocity, [L $T^{-1}$] |
| $V^*$ | velocity constant, [L $T^{-1}$] |
| $V_d$ | shear force, [M L $T^{-2}$] |
| $V_R$ | punching shear strength, [M L $T^{-2}$] |
| $X$ | penetration depth, [L] |
| $\ddot{X}$ | penetration acceleration, [L $T^{-2}$] |

*Greek lower case*

| | |
|---|---|
| $\beta$ | shear modulus retention factor, [−] |
| $\gamma$ | concrete dilatation angle, [−] |
| $\delta$ | crack separation, [L] |
| $\dot{\varepsilon}$ | strain-rate, [$T^{-1}$] |
| $\mu$ | co-efficient of friction, [−] |
| $\nu$ | Poisson's ratio, [−] |
| $\rho$ | flexural reinforcement ratio, [−] |
| $\rho_c$ | concrete density, [M $L^{-3}$] |
| $\rho_v$ | shear reinforcement ratio, [-] |
| $\sigma_{ca}$ | concrete aggregate interlock normal stress, [M $L^{-1}$ $T^{-2}$] |
| $\sigma_{ct}$ | concrete tensile stress, [M $L^{-1}$ $T^{-2}$] |
| $\sigma_p$ | cement paste plasticisation stress, [M $L^{-1}$ $T^{-2}$] |
| $\tau_{ca}$ | concrete aggregate interlock shear stress, [M $L^{-1}$ $T^{-2}$] |
| $\varphi(x)$ | slab deformed configuration shape function, [−] |
| $\phi$ | reinforcement bar diameter, [L] |
| $\psi$ | slab rotation, [−] |
| $\psi_R$ | slab rotation at failure, [−] |

constituents of RC structures, namely the concrete and the steel reinforcement.

*1.2.1. Concrete properties*

It has been shown by many researchers (e.g. Refs. [3–11]) that the tensile and compressive strengths of concrete both increase with loading rate. A very comprehensive review of experimental data in this respect has been carried out by Cotsovos and Pavlović [12].

The 1990 and 2010 Model Codes [1,13,14] provide relationships which give the increase in strength and modulus with strain-rate. These relationships are valid for strain rates up to 300/s covering low to moderate impacts. The increases in compressive ($f_c$) and tensile ($f_t$) strengths are given by (1) and (2) respectively as:

$$\frac{f_{c,dynamic}}{f_{c,static}} = \begin{cases} \left(\dfrac{\dot{\varepsilon}}{30\times10^{-6}}\right)^{0.014}, & \dot{\varepsilon} \le 30/s \\ 0.012\left(\dfrac{\dot{\varepsilon}}{30\times10^{-6}}\right)^{\frac{1}{3}}, & 30/s \le \dot{\varepsilon} \le 300/s \end{cases} \quad (1)$$

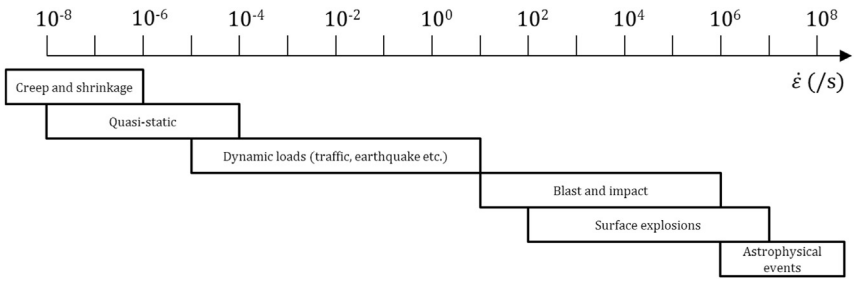


**Fig. 1.** Strain-rate ranges for various load sources (after [1]).

$$\frac{f_{ct,dynamic}}{f_{ct,static}} = \begin{cases} \left(\frac{\dot{\varepsilon}}{1\times10^{-6}}\right)^{0.018}, & \dot{\varepsilon} \le 10/s \\ 0.0062\left(\frac{\dot{\varepsilon}}{1\times10^{-6}}\right)^{\frac{1}{3}}, & 10/s \le \dot{\varepsilon} \le 300/s \end{cases} \quad (2)$$

An increase in the fracture energy, $G_F$, with increasing loading rate was also observed by other researchers [5,15–18], although as stated in Refs. [1,13] further work is needed in this area.

#### 1.2.2. Steel reinforcement properties

The effect of loading rate on metallic materials, such as steel, is another well-known phenomenon and literature (e.g. Refs. [19,20]) confirms the increase of steel reinforcement yield stress with loading rate. Various material models, such as the Johnson and Cook [21] or the Cowper and Symonds [22] models are used to take into account the dynamic effects in the constitutive behaviour of steels.

### 1.3. Effect of high loading rates on structural response

The loading rates which structures undergo as a result of severe blast and impact threats can be significantly larger than those due to static loading as suggested by Fig. 1.

Indeed, the Model Code 2010 [1,13] recommends that dynamic effects such as mass and resonance effects are considered. It also suggests paying attention to damage mechanisms such as spalling and scabbing and, in particular, attention to formation of shear plugs due to punching shear failure.

Since this paper is principally aimed at investigating the response of RC flat slabs subjected to impact (rather than blast) loading, a brief review of experimental and numerical work related to this subjected is included in this section.

Various researchers (e.g. Refs. [23–39]) have carried out work related to drop impact loadings on RC beams and slabs and the principal ones are discussed hereunder.

#### 1.3.1. Beams

Hughes and Beeby [23] observed that shear failure may occur in RC beams due to activation of higher modes under dynamic loading.

Saatci and Vecchio [33] carried out impact tests on RC beams and concluded that shear mechanisms are typically critical in such scenarios, even in the case of beams which are flexure-critical under static load conditions. A similar observation was made by Ožbolt & Sharma [37] and Magnusson et al. [40,41], who have shown that RC beams which failed in a ductile (flexural) manner under static loading changed to a brittle (shear) failure when subjected to impact loading or air blast explosions in a shock tube. Abbas et al. [34] also observed an increase in the load-carrying capacity and stiffness of beams subjected to impact loading when compared to the members' static capacities.

Cotsovos et al. [30,35] concluded that in RC beams subjected to impact loading, the effect of the inertial loads on the response leads to an increase in the member stiffness and its load-carrying capacity. This increase in stiffness is taken into account by considering a reduced span which decreases with increasing loading rate, based on the member's dynamic characteristics (shear wave speed and limiting moment-carrying capacities) and the loading rate.

Thus, the increase in stiffness observed in such cases of dynamic loading are attributed to the delayed crack formation due to the enhanced tensile strength resulting from high strain-rate effects, the effects of inertial forces or a combination of the two phenomena.

#### 1.3.2. Slabs

Experimental and numerical work on RC slabs carried out by Miyamoto et al. [25,26] demonstrated that shear mechanisms dominate the behaviour of RC structures subjected to impulsive loads and an increase in loading rate is linked with an increase in the failure load, as shown in Fig. 3. Miyamoto et al. also proposed a failure envelope for slabs subjected to impact loading, shown in Fig. 2. It was also reported a transition of failure mode from flexural-punching to punching shear with increasing the loading rate as shown in Fig. 2.

Saito et al. [27] also observed an increase in the failure load of various RC structural systems subjected to high speed loading when compared with the elements' corresponding static load capacities. A change in the deformation and failure mode were also observed.

Delhomme et al. [28] observed from drop tests on RC slabs that during the very initial stage of impact when the impactor is in contact with the slab, there is a reduced radius of the slab which shows bending behaviour. This leads to an increase in stiffness of the slab, which is similar to the phenomenon discussed by Cotsovos et al. [30,35] and Hughes and Beeby [23].

### 1.4. Modelling dynamic structural response of RC structures

Without having to rely on costly large-scale testing of prototypes, the structural engineer often needs to be able to predict the load-carrying capacity of a RC structure subjected to dynamic loading. The alternative methods are use of numerical techniques (e.g. non-linear finite element analysis) or analytical methods (e.g. mass-spring models). The former are often difficult to employ in practical applications due to their computational cost and software package limitations in handling, for example, concrete cracking.

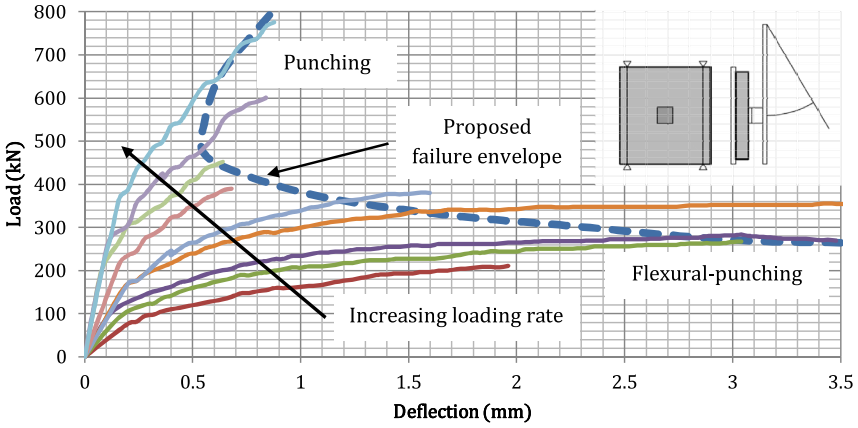


**Fig. 2.** Load-deflection response and failure envelope proposed by Miyamoto et al. (after [25,26]); slab dimensions 1.3 × 1.3 × 0.13 m with loading plate 150 × 150 mm.

Thus, the use of analytical and simple mass-spring models is favoured for practical use and various models have been proposed, discussed hereunder.

Abdel-Rohman and Sawan [42,43] proposed various analytical methods to estimate the dynamic response of RC slabs subjected to impact loading, with good correlation with test data being observed. The authors make use of the Petry formula to estimate the impact force and contact time. The Petry formula, originally developed in 1910, is given by:

$$X = KARV' \tag{3}$$

where $X$ is the penetration of the impactor into the slab, $K$ is a material constant given as $2.97 \times 10^{-2}$ m$^3$/kN for reinforced concrete, $A$ is the impactor section pressure, $R$ is a penetration ratio and $V$' is a velocity factor given by:

$$V' = \log\left(1 + \left[\frac{V_0}{V^*}\right]^2\right) \tag{4}$$

where $V_0$ is the initial velocity of the impactor and $V^*$ is a constant given by 141.33 m/s. Further discussion of this formula, its parameters and its use is given in Section 3.1.

Historically, the CEB Bulletin 187 [44] was an early attempt in modelling the response of RC slabs subjected to impulsive loading and potential punching failure by a mass-dashpot-spring model, as shown in Fig. 3. This model assumes two masses, one local mass corresponding to the impactor and the punching shear cone and another mass corresponding to the slab. The main limitation of this model is that it assumes that the formation of the punching cone is governed by the tensile stress in the concrete, dowel action and shear resisted by the stirrups whereas in reality the punching strength is also influenced by the slab deformation [13]. This implies that the stiffness $R_2$ (Fig. 2) depends on the deflection $w_1$ and not only on $(w_2 - w_1)$ as assumed in Ref. [44]. In addition, for cases where failure does not occur even if the tensile capacity is exceeded, the CEB Bulletin attributes this fact to the scatter in concrete's tensile strength, rather than to the stiffness and/or strength increase due to dynamic and strain-rate effects.

A significantly improved model to assess the flexural response of RC slabs during and after impact was proposed by Delhomme [28,45], where the response was assumed to be split into two phases, viz. the contact phase and the post-contact phase.

In the former, the slab mass and stiffness are based on a reduced radius (thus increased stiffness), from which the contact load and energy transmitted to the slab are obtained. These are then used as initial conditions for the post-contact model, where the slab undergoes free vibration and its response is obtained. However, in this case, the model parameters are obtained from experimental data and/or numerical models of the impact test and no information on capacity and/or failure is obtained from the model.

Barbier and Roby [46] used a similar concept where the mass and stiffness are functions of time but the model parameters are obtained from curve fitting to numerical results.

In addition, these models provide only information on the response (i.e. the shear demand) and there is no information about the shear strength capacity or whether failure occurs or not.

### 1.5. Aim of current study

Thus, the aim of the current study is to develop a model which can be used to predict the dynamic response of RC slabs subjected to impact loading which does not rely on obtaining model parameters from experimental results or numerical simulations and which follows an integral approach in which both the loading on the structure (shear demand) as well as its capacity (shear strength supply) are predicted.

Consideration of strain-rate effects will be made in both aspects of the problem and this will lead to assessing the relative significance of the strain-rate effects and the initial increased stiffness of the structure associated with inertial effects.

The model can then be used to predict the slab's behaviour and likelihood of failure due to punching shear and also provide

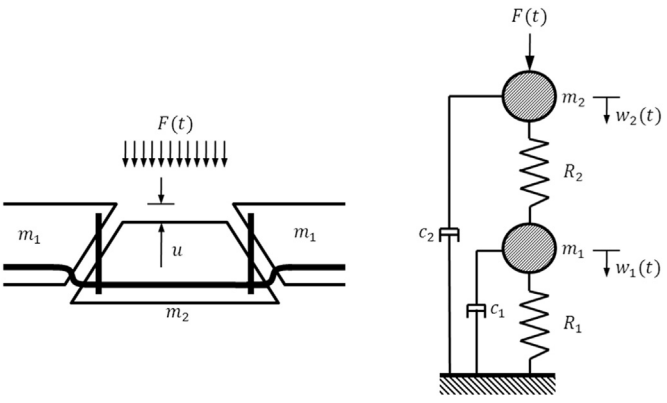


**Fig. 3.** CEB 187 model for punching shear failure (after [44]).

information about the levels of deformation at failure. The application is illustrated by various case studies RC slabs with and without transverse reinforcement and low to moderate impacts.

It should be noted at this point that the source of impact loadings being considered in this paper is due to impactors which are relatively rigid and thus non-deformable (e.g. impulsive axial load in column such as in a progress collapse scenario, falling debris on a slab, falling objects on a slab and rock falls); such impact loadings are termed as 'hard impacts' in the CEB Bulletin 187 [44] and in this case it is assumed that the kinetic energy imparted by the impactor is entirely absorbed by the deformation of the struck body, i.e., the RC slab.

### 1.6. Presentation of current study

Following this introduction, the fundamentals of the critical shear crack theory will be discussed and how this is extended to take into account the effects of strain-rate on punching shear capacity. Section 3 will present a mass-spring-damper model to predict the flexural deformation response of a RC slab subjected to an impact load and the use of this model to investigate various slab systems will be presented in Section 4. Finally, the main findings and merits of this paper will be summarised in Section 5.

## 2. Dynamic punching shear strength

### 2.1. The critical shear crack theory

Punching is a brittle form of failure observed in RC flat slab structures, typically at slab-column connections but also observed in many drop impact tests.

The punching capacity of slab systems has been investigated since the 1950s but most strength models presented in design codes are empirically derived e.g. the American ACI 318-08 [47], the British BS 8110-1 [48] and the European EC 1992-1 [49].

A physically-based mechanical model was proposed in 1988 by Muttoni [50] and subsequently formed the basis for punching shear provisions in various Swiss codes and also in the latest version of the Model Code [1,13].

The model is based on the critical shear crack theory (CSCT) and assumes that the shear strength is governed by the width and the roughness of a shear crack which develops through an inclined compression strut which carries the shear force, as shown in Fig. 4.

Assuming that the crack width, $w$, is proportional to the slab rotation, $\psi$, the shear strength is calculated from a set of assumed kinematics characterised by the rotation of the slab and by integrating the contribution of the concrete tensile stresses and the aggregate interlock along the failure surface. Most of the shear stress is transferred at the bottom end of the crack where the crack width is small while any contribution from dowel action of the reinforcement is ignored due to the expected spalling of the concrete cover.

It can be shown that the punching shear capacity decreases with increasing rotation since this implies wider cracks, thus reducing both tensile and aggregate contributions. Further details can be found in Muttoni and Fernández Ruiz [51,52] for slabs with no transverse reinforcement and Fernández Ruiz and Muttoni [53] for slabs with transverse reinforcement, as well as for non-symmetrical cases investigated by Sagaseta et al. [54].

For design purposes, rather than evaluating the contributions of concrete tension and aggregate interlock discretely for individual cases, a failure criterion was proposed [51] to cover most practical geometric and material configurations, given in SI units (N, mm) by:

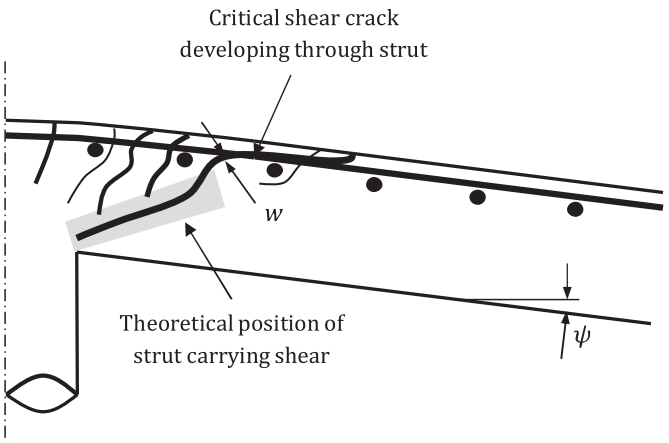


**Fig. 4.** Critical shear crack through compression strut (after [51]).

$$\frac{V_R}{b_0 d_v \sqrt{f_c}} = \frac{0.75}{1 + \frac{15\psi d}{d_{g0}+d_g}} \tag{5}$$

where $V_R$ is the punching shear capacity, $d$ is the effective depth of the slab, $b_0$ is the control perimeter at $(d/2)$ from the edge of the support, $d_v$ is the shear-resisting effective depth, $d_g$ is the maximum aggregate size in the concrete and $d_{g0}$ is a reference aggregate size taken as 16 mm.

Knowing the load-rotation response of a particular slab, then the punching shear capacity, $V_R$, and the deformation (rotation) at failure, $\psi_R$, can be immediately established by the intersection of the two curves, as shown in Fig. 5.

In the case of slabs with transverse (shear) reinforcement, the contribution from the steel reinforcement (which varies with rotation due to the varying crack width and thus varying stress in the shear reinforcement) is added to the concrete contribution, using expressions given in Refs. [1,13,53] to give a new failure criterion, as shown schematically in Fig. 6.

The aim is to extend this formulation to take into account the dynamic enhancement of the concrete properties, as discussed in Section 1.2.1, by considering the two main constituents of punching capacity in turn (i.e. tensile stress in the concrete and aggregate interlock). The dynamic effects on the load-rotation response will then be considered in Section 3 to produce a plot similar to Fig. 5 (or Fig. 6) for the dynamic case.

### 2.2. Influence of strain-rate on fracture toughness

Concrete subjected to tension initially follows a linear elastic stress–strain response, which response is limited by a stress value

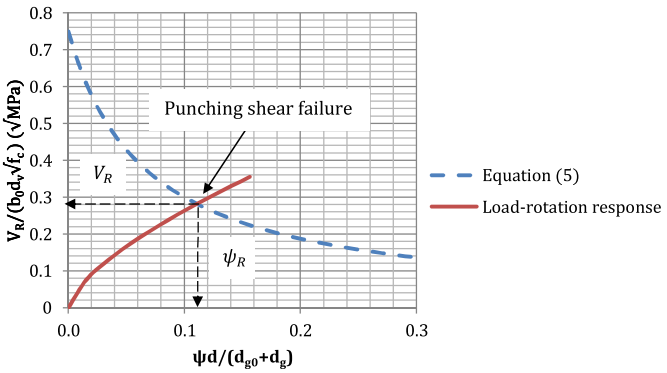


**Fig. 5.** Evaluation of punching shear capacity (unreinforced).

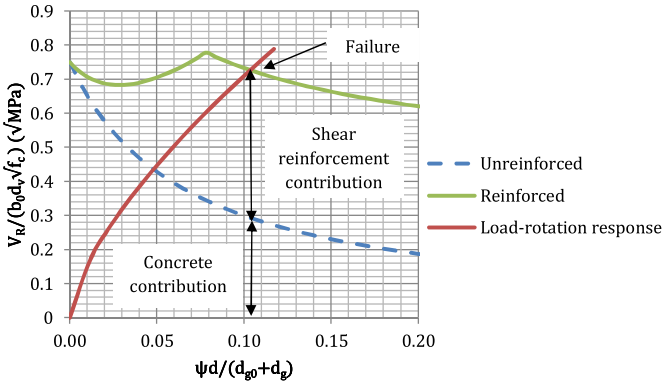


**Fig. 6.** Evaluation of punching shear capacity (reinforced).

of $f_{ct}$, after which a crack forms. Following the formation of the crack, softening behaviour occurs, until a maximum crack separation, $w_c$, is reached when there is complete separation of the two crack faces. This is further explained by Hillerborg et al. [55].

Various models have been proposed to describe the softening behaviour. One such model is that put forward by Hordijk [56], who gives an expression for the stress–displacement variation after the initial crack formation as:

$$\sigma_{ct}/f_{ct} = \left(1+\left\{c_1\frac{w}{w_c}\right\}^3\right)e^{-\frac{c_2 w}{w_c}} - \frac{w}{w_c}\left(1+c_1^3\right)e^{-c_2} \tag{6}$$

where $c_1$ and $c_2$ are constants given by 3 and 6.93 respectively.

Hordijk also gives an expression for the crack separation displacement as:

$$w_c = 5.14\frac{G_F}{f_{ct}} \tag{7}$$

The energy dissipated in opening the crack, $G_F$, or fracture energy, is given by the area underneath the stress–displacement curve, or the integral of (6) over $w_c$ as:

$$G_F = f_{ct} w_c\left[\frac{1}{c_2}\left\{1+6\left(\frac{c_1}{c_2}\right)^3\right\} - e^{-c_2}\left\{\frac{1}{c_2}+c_1^3\left(\frac{1}{c_2}+\frac{3}{c_2^2}+\frac{6}{c_2^3}+\frac{6}{c_2^4}\right)+\frac{1}{2}\left(1+c_1^3\right)\right\}\right] \tag{8}$$

For $f_c$ not exceeding 80 MPa, Model Code 1990 [14] gives an expression for $G_F$ as:

$$G_F = G_{F0}\left(\frac{f_c}{f_{c0}}\right)^{0.7} \tag{9}$$

where $G_{F0}$ is a reference fracture energy (which is a function of $d_g$) and $f_{c0}$ is a reference compressive strength, given as 10 MPa.

It should be noted that Model Code 2010 [1,13] gives a simplified expression in which $G_F$ varies only with $f_c$ and constant with $d_g$, as shown in Fig. 7. In this paper, the expression found in Model Code 1990 will be used, since this, in the opinion of the authors, this is more general.

While the expression given by (6) was proposed by Hordijk based on the static response of concrete, Weerheijm and Van Doormaal [9] postulate that the same equation can be used to describe the softening behaviour even in the dynamic case.

Knowing the variation of $G_F$ with $f_c$ and noting that $f_{ct} = 0.3\sqrt[3]{f_c^2}$, it is possible to express the variation of $G_F$ and $w_c$ with strain-rate, by using the rate-dependent concrete strengths given by (1) and (2) with $f_c$ in MPa. These are given by (10) and (11) respectively.

$$G_F(\dot{\varepsilon}) = \begin{cases} 0.221 G_{F0} f_c^{0.7}\dot{\varepsilon}^{0.0098}, & \dot{\varepsilon} \le 30/s \\ 0.103 G_{F0} f_c^{0.7}\dot{\varepsilon}^{0.2333}, & 30/s \le \dot{\varepsilon} \le 300/s \end{cases} \tag{10}$$

$$w_c(\dot{\varepsilon}) = \begin{cases} 2.97 G_{F0} f_c^{\frac{1}{30}}\dot{\varepsilon}^{-0.0082}, & \dot{\varepsilon} \le 30/s \\ 2.85 G_{F0} f_c^{\frac{1}{30}}\dot{\varepsilon}^{-0.1}, & 30/s \le \dot{\varepsilon} \le 300/s \end{cases} \tag{11}$$

The dynamic increase factor for the fracture toughness $G_F/G_{F0}$ given by expression (10) is of similar magnitude to that obtained by Oh [18]; for concrete strengths around 30 MPa the difference between the predictions of $G_F/G_{F0}$ given by both approaches is 20%.

Using these relationships and equating (8) to (9), it is also possible to obtain strain-rate-dependent values ($\dot{\varepsilon}$ in 1/s) for the constants $c_1$ and $c_2$ as:

$$c_1(\dot{\varepsilon}) = 6.8 - 0.0061\dot{\varepsilon} \tag{12a}$$

$$c_2(\dot{\varepsilon}) = 2.7 - 0.0071\dot{\varepsilon} \tag{12b}$$

Fig. 8 shows the effect of strain-rate on the tensile strength and fracture toughness as described by the rate-dependent form of (6) for various strain-rate values ranging from 10 to 300/s, representing low to moderate impact loadings.

### 2.3. Influence of strain-rate on aggregate interlock

After concrete cracks, it nonetheless still has the capacity to transmit shear ($\tau_{ca}$) and normal ($\sigma_{ca}$) stresses across the crack surfaces by means of aggregate interlock action, described graphically in Fig. 9.

Following the initial crack opening, $w_0$, the displacements of the crack surfaces in terms of the successive crack translation, $\delta$, are given by:

$$w = w_0 + \delta\sin\gamma \tag{13a}$$

$$v = \delta\cos\gamma \tag{13b}$$

where $\gamma$ is the dilatation angle taken as 27° [57].

These are shown in Fig. 10.

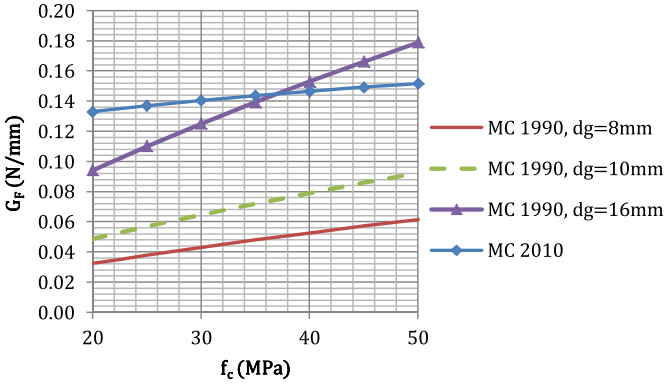


**Fig. 7.** Variation of $G_F$ with $f_c$.

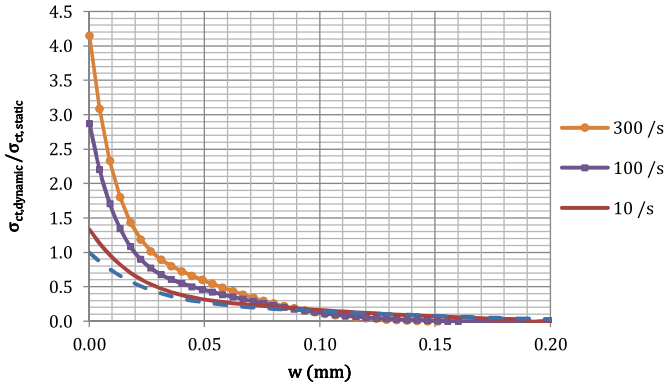


**Fig. 8.** Variation of $\sigma_{ct}$ with $\dot{\varepsilon}$.

The aggregate interlock strength component can be evaluated by using various physically-based or empirically-derived models.

In this paper, this is done by using the physical model proposed by Walraven [58] and extended by Guidotti [57], where the two stress components are evaluated along the unit crack area as:

$$\sigma_{ca} = -\sigma_p\left(\overline{A}_x - \mu\overline{A}_y\right) \le 0 \tag{14a}$$

$$\tau_{ca} = \sigma_p\left(\mu\overline{A}_x + \overline{A}_y\right) \tag{14b}$$

where $\mu$ is the co-efficient of friction between the aggregate granules and the cement paste (taken as 0.4) and $\sigma_p$ is the cement paste plasticisation stress in MPa, given by:

$$\sigma_p = 6.39 f_c^{0.56} \tag{15}$$

By idealising the aggregate particles as spheres, as shown in Fig. 11, the projected contact areas, $\overline{A}_x$ and $\overline{A}_y$, are derived (Ref. [58]) from the probability distributions of an aggregate particle of a specific size (limited by $d_g$) being present along the crack.

The crack contact surface areas are obtained by numerical means for various crack kinematics describing different crack widths. Further details can be found in Refs. [57] and [58]. Assuming that $\sigma_p$ varies with strain-rate according to (1), then the dynamic aggregate interlock strength can be evaluated for various cases.

### 2.3.1. Comparison with test data

The extension of Walraven's aggregate interlock model taking into account strain-rate effects is verified by comparison with test results from experiments carried out on dynamic push-off tests

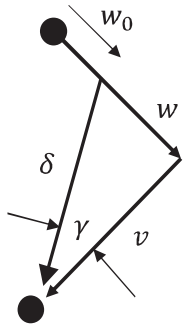


**Fig. 10.** Initial and final crack translations (after [57]).

carried out by Lui [59]. For unreinforced specimens loaded at 10,000 MPa/s (or $\dot{\varepsilon}$ approximately equal to 0.3/s), Lui measured a limiting strength of 8.75 MPa. Using Walraven's model and applying the strain-rate enhancement to $\sigma_p$, the maximum stress predicted is 7.36 MPa, which is a very good approximation to the measured value.

The small difference between the predicted and observed strengths could be attributed to the fact that the value of $\mu$ adopted is the same as for the static case. Although it is debatable as to whether $\mu$ also increases with $\dot{\varepsilon}$, in the lack of a statistically-significant result database, it is not possible to confirm this assertion at this stage. Thus, a value of $\mu = 0.4$ will be used throughout this paper.

### 2.4. Dynamic punching shear failure criterion

Having established strain-rate-dependent expressions for the two main components of punching shear capacity, it is now possible to obtain the capacity for any slab configuration.

It has been shown [51] for the static case that 99 experimental results fall within a very narrow region covering many practical slab and column geometries and slab reinforcement ratios, as shown in Fig. 12.

Experimental results from various tests at high-rate loading also suggest that the results fall within a similar relatively narrow failure region which however lies above the average failure criterion given by (5). This is shown in Fig. 13.

Thus, it is necessary to establish such a region for the dynamic case and propose a dynamic failure criterion similar to (5).

For this purpose and knowing the relative sensitivity of the various parameters from Refs. [57], three slab configurations (all having $f_c = 30$ MPa and a cover of 25 mm) were chosen, outlined in Table 1.

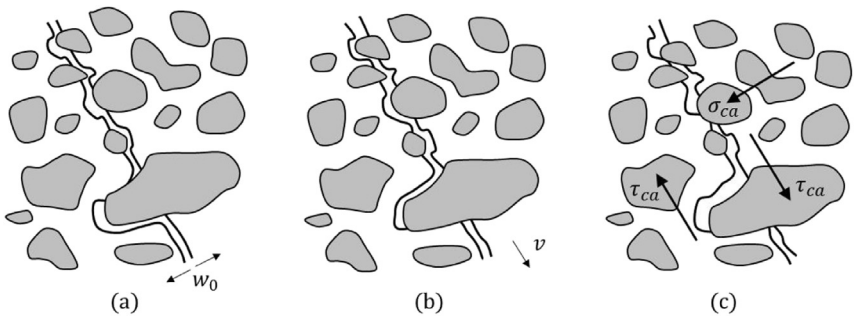


**Fig. 9.** Aggregate interlock action: (a) initial crack opening due to tension; (b) longitudinal sliding reinstating contact between crack faces; (c) crack kinematics and generation of normal and shear stresses.

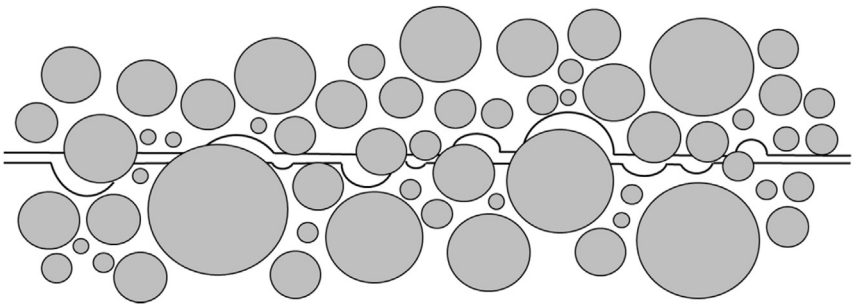

**Fig. 11.** Idealisation of aggregate particles into spheres (after [58]).

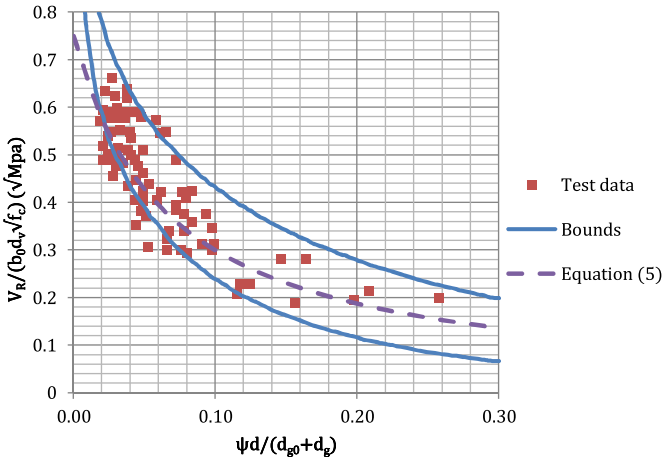


**Fig. 12.** Punching shear failure region for static loads as a function of critical shear crack width (after [51]).

Assuming a crack inclination angle of 45°, a discrete crack model was derived for each case. In each case, for different slab rotation values and crack separations, the normal and shear forces along the crack surface (shown in Fig. 14) were evaluated using:

$$N = \int_{A_{cr}} (\sigma_{ct} + \sigma_{ca}) dA \tag{16a}$$

$$S = \int_{A_{cr}} \tau_{ca} dA \tag{16b}$$

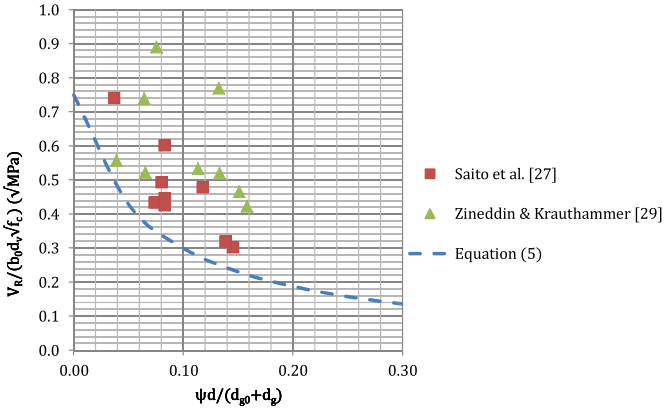


**Fig. 13.** Punching shear failure results from various high-rate tests.

Thus, the total shear force that could be carried by the crack was found:

$$V_R = \frac{N+S}{\sqrt{2}} \tag{17}$$

An illustration of the force variation with crack translation is shown in Fig. 15.

Thus, for each value of rotation, the maximum shear force that the slab can carry is found, enabling a plot similar to Fig. 12 to be derived. The resulting failure region (for the static) case matches closely the region shown in Fig. 12.

The procedure was repeated for different $\dot{\varepsilon}$ values (10/s, 100/s and 300/s) and the results are shown in Figs. 16 to 18.

These results clearly suggest that the punching shear strength increases with strain-rate, with a particular increase observed at low rotation values and most significant at the larger strain-rate values. From these results, a modified expression for the failure criterion is proposed in each case, viz.:

$$\frac{V_R}{b_0 d_v \sqrt{f_c}} = \frac{0.8}{1 + \frac{15\psi d}{d_{g0}+d_g}} \text{for} \dot{\varepsilon} = 10/\text{s} \tag{18}$$

$$\frac{V_R}{b_0 d_v \sqrt{f_c}} = \frac{1}{1 + \frac{15\psi d}{d_{g0}+d_g}} \text{for} \dot{\varepsilon} = 100/\text{s} \tag{19}$$

$$\frac{V_R}{b_0 d_v \sqrt{f_c}} = \frac{1.3}{1 + \frac{15\psi d}{d_{g0}+d_g}} \text{for} \dot{\varepsilon} = 300/\text{s} \tag{20}$$

Although further experimental data is required to verify the above proposed failure criteria, the results suggest that while at the lower strain-rates the increase from the static case is only by 7%, for strain-rates of 100 and 300/s, the respective increases are 33% and 73%, which are very significant. For strain-rates higher than 300/s, which can be the case in ballistic problems, the strain-rate dependent relationships for the materials used in the model and the contribution of aggregate interlock would need to be reviewed to consider additional mechanisms such as aggregate crushing.

**Table 1**
Slab scenarios considered for discrete crack models.

| | Case 1 | Case 2 | Case 3 |
|---|---|---|---|
| $\rho$ (%) | 0.5 | 1 | 1.5 |
| $\phi$ (mm) | 12 | 16 | 25 |
| $h$ (mm) | 200 | 200 | 250 |
| $r_c$ (mm) | 150 | 150 | 200 |
| $d_g$ (mm) | 16 | 16 | 32 |

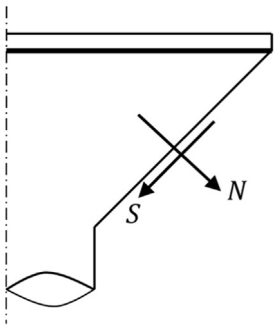


**Fig. 14.** Punching shear strength components.

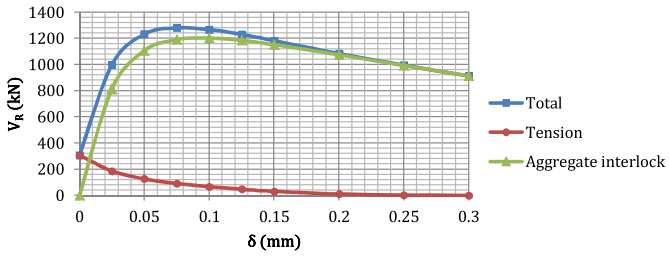


**Fig. 15.** Strength contributions from tension and aggregate interlock (Case 1, slab rotation = 0.001).

## 3. Prediction of dynamic flexural response

The discussion in Section 2 was concerned with the shear capacity of flat slabs in the case of dynamic loading.

In this section, the response of a slab when subjected to an impact loading will be investigated. Thus, the slab's displacement (and hence rotation) are obtained and the load-rotation response is used in conjunction with the failure criterion discussed in Section 2.

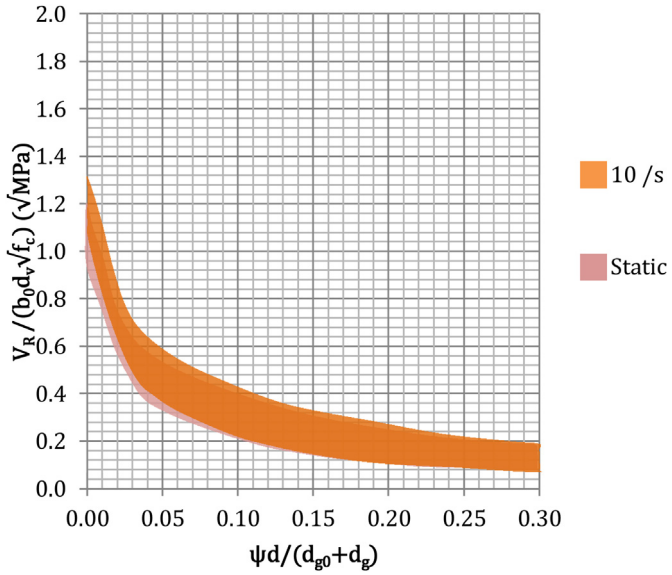


**Fig. 16.** Failure regions for Cases 1–3 (static and 10/s).

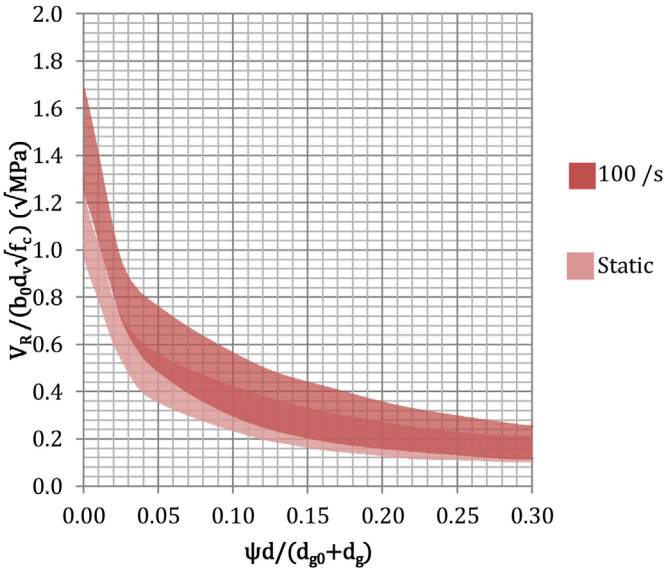


**Fig. 17.** Failure regions for Cases 1–3 (static and 100/s).

### 3.1. Modelling the impact event

In this work, it is assumed that the loading source is an impactor of known mass, $m_i$, and radius, $R_i$, which is dropped from a known height, $h_i$, thus having an initial velocity equal to $2gh_i$ from simple energy conservation considerations.

In order to determine the impact force, $P(t)$, imparted to the slab, it is necessary to determine the contact time, $t_c$, and the acceleration of the impactor's penetration into the slab, from which the contact force is then easily obtained.

From Newton's second law of motion:

$$P(t) = m_i \ddot{X} = m_i V \frac{dV}{dX} \tag{21}$$

where $\ddot{X}$ is the acceleration of the impactor's penetration and $V$ is the velocity of penetration.

Using the Petry formula described by (3) and using (4), then it can easily be shown through some algebraic manipulation that (21) may be written as:

$$\ddot{X} = aXe^{bX^2} \tag{22}$$

where the constants $a$ and $b$ are given by:

$$a = \frac{2.3\pi R_i (V^*)^2}{m_i KR} \tag{23a}$$

$$b = \frac{4.6\pi R_i}{m_i KR} \tag{23b}$$

It is obvious that (22) is a non-linear non-homogenous ordinary differential equation and it can be solved by numerical means (in this work, the fourth-order Runge–Kutta method was employed), subject to the initial conditions $X = 0$ and $\dot{X} = V_0 = \sqrt{2gh_i}$ at $t = 0$.

The contact time is represented by the time required for $\dot{X}$ to become zero.

The constant $R$ in (3) and (23) is the penetration ratio, representing the penetration into a slab of finite thickness to the penetration into a slab of infinite thickness.

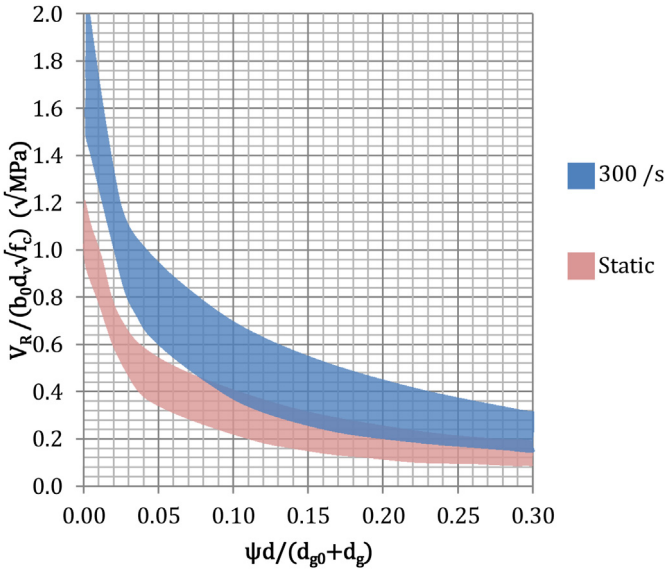


**Fig. 18.** Failure regions for Cases 1–3 (static and 300/s).

Thus, $R = 1$ represents an infinitely thick slab. Abdel-Rohman and Sawan [42,43] suggest using $R = 1.1$ or 1.2 for typical RC slab thicknesses to obtain more realistic results.

This was verified by means of the following parametric study based on results reported by Delhomme et al. [28,45]. Delhomme et al. dropped a 450 kg mass from a height of 30 m on a 0.28 m thick slab and measured a contact time of 3.5 ms and a maximum contact force of 5 MN. Modelling this loading scenario, the contact time and force were evaluated for various values of $R$, summarised in Table 2.

It can be observed that a good correlation with experimental results is obtained for the case of $R = 1.1$, suggesting that the Petry formula can be used to provide a simple yet accurate method of estimating the contact time and contact force history for typical RC slab applications.

### 3.2. Modelling the slab response

Knowing the contact time, it is now possible to develop a simplified mass-spring-dashpot model to simulate the impact on an RC flat slab. For this purpose, a two-phase model is proposed, based on the model developed by Delhomme et al. [28,45] and shown graphically in Fig. 19.

In the initial phase, the impactor is in contact with the slab between $t = 0$ and $t = t_c$. The slab parameters are based on an initial reduced slab radius, leading to an increased geometric stiffness, $k_{s0}$, and a reduced slab mass, $m_{s0}$. The dashpot, $c_{s0}$, represents the slab's dissipating action while the contact stiffness, $k_c$, is set such that $u_i(t_c) = u_s(t_c)$. At the end of this phase, the slab displacement and energy are obtained and these are used as initial conditions for the next phase, during which the slab mass, $m_s$, stiffness, $k_s$ and dashpot, $c_s$, are based on the actual slab geometry, giving the complete slab response.

**Table 2**
Contact results for various $R$ values.

| $R$ | $t_c$ (ms) | $P_{max}$ (MN) |
|---|---|---|
| 1.0 | 3.41 | 5.14 |
| 1.1 | 3.57 | 4.91 |
| 1.2 | 3.73 | 4.7 |

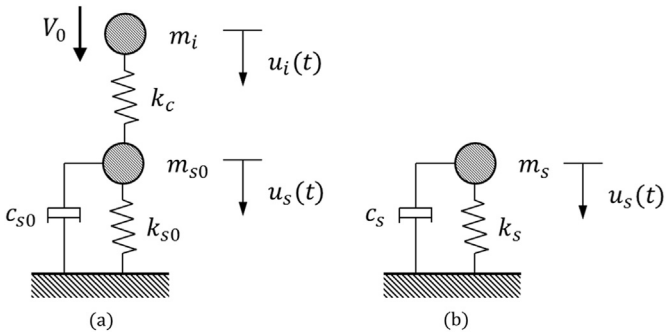


**Fig. 19.** Two-phase model: (a) Contact phase; (b) Post-contact phase.

These two phases are described in further detail in Sections 3.2.1 and 3.2.2 respectively.

#### 3.2.1. Contact phase

The various model parameters are outlined below.

– Slab stiffness

As discussed in Section 1.3, experimental and numerical results suggest that during the initial response of a slab subjected to an impact event, an increased stiffness is observed. In this paper, the increase in stiffness is modelled by considering a reduced slab geometry or radius, $r_{s0}$, on the basis of which the flexural stiffness is computed.

The evaluation of $r_{s0}$ is based upon the $L_{eff}$ concept proposed by Cotsovos et al. [30,35], whereby it is assumed that immediately after contact in the case of high-rate loading, a reduced portion of the full span reacts to the applied load. While Cotsovos developed the concept for RC beams, similar observations were made by Delhomme et al. [28,45] for the case of RC slabs.

This reduced span (termed $L_{eff}$ by Cotsovos) is limited by the load-carrying capacity based on the lower part of the RC section ($M_{Rd}$) and upper part of the RC section ($M'_{Rd}$), suggesting that the slab behaves essentially as a fixed-ended member irrespective of its actual boundary conditions, as shown graphically in Fig. 20.

The moment capacity for a RC section is obtained from simple equilibrium and is given by:

$$M_{Rd} = \rho d^2 f_y \left(1 - \frac{\rho f_y}{2 f_c}\right) \tag{24}$$

where $\rho$ is the reinforcement ratio at the level being considered (top or bottom) and $f_y$ is the steel reinforcement yield stress.

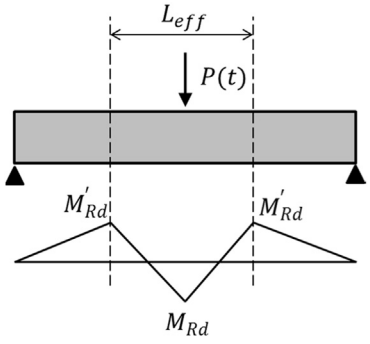


**Fig. 20.** Definition of $L_{eff}$ (after Cotsovos [30,35]).

The limiting moment capacity at the top of the section is either the moment capacity which can be generated by any reinforcement present at the top of the section as determined by (24) or the section's cracking moment ($M_{cr}$) for the case of a section of thickness $h_s$ with no top reinforcement, given by:

$$M_{cr} = \frac{f_{ct} h_s^2}{6} \tag{25}$$

Defining the velocity, $v_c$, at which shear waves travel through concrete as:

$$v_c = \sqrt{\frac{G_c}{\rho_c}} \tag{26}$$

where $G_c$ is the concrete shear modulus and $\rho_c$ is the concrete density, it is possible to find the time, $\Delta t$, required to reach the limiting moment capacities as per Fig. 20 as:

$$\Delta t = \frac{L_{eff}}{2 v_c} \tag{27}$$

Defining $P'$ as the load required for $M'_{Rd}$ to be generated at the slab's upper face, then.

$$P' = \frac{8 M'_{Rd}}{L_{eff}} \tag{28}$$

If $\dot{P}$ is the loading rate (obtained from the Petry formula as described in Section 3.1), then $P'$ is simply given by $\dot{P}\Delta t$. Using this expression, (27) and (28), $L_{eff}$ is found as.

$$L_{eff} = \frac{M'_{Rd} v_c}{\dot{P}} \tag{29}$$

Thus, from (29), $L_{eff} \propto 1/\dot{P}$ for any given section, confirming physical observations that the stiffness is observed to increase (i.e. $L_{eff}$ decreases) with increasing loading rate.

From the value of $L_{eff}$, $r_{s0}$ can easily be found purely from geometric considerations. Two limiting cases are identified, viz. the case with no top reinforcement and the case where the top and bottom reinforcement are equal, shown in Fig. 21. In the latter case, the limiting moment is $M_{cr} \ll M_{Rd}$ and thus may be ignored.

This leads to the following range for $r_{s0}$:

$$\frac{L_{eff}}{2} \le r_{s0} \le L_{eff} \tag{30}$$

Model Code 2010 [1,13] gives expressions for the load-rotation response of a RC slab by using the levels of approximation method [60]. In this instance, a Level II approximation is used, whereby the load-rotation relationship is given by:

$$\psi = \frac{3}{2} \frac{r_s}{d} \frac{f_y}{E_s} \left( \frac{M_{sd}}{M_{Rd}} \right)^{3/2} \tag{31}$$

where $r_s$ indicates the position of zero radial bending moment with respect to the support axis (typically taken as $\approx 0.22L$ for flat slabs of span $L$), $E_s$ is the elastic modulus of steel reinforcement, $M_{sd}$ is the average bending moment per unit length in the slab's column (support) strip and $M_{Rd}$ is the average flexural strength per unit length in the column strip, given by (24).

The various terms in (31) affect the crack width (and thus the rotation). The term $(r_s/d)$ represents the slenderness of the slab while the term $(M_{sd}/M_{Rd})$ is the bending moment demand ratio. The strain in the reinforcement at yielding is considered by the term $(f_y/E_s)$.

For internal columns, from the Model Code [1,13], $M_{sd}$ is related to the load $V_d$ by:

$$M_{sd} = \frac{V_d}{8} \tag{32}$$

Substituting (32) and the appropriate value of $r_{s0}$ into (31) leads to a simple expression for load-displacement and hence its gradient to give the slab stiffness, $k_{s0}$.

– Slab mass

From the computed $L_{eff}$, it is also possible to work out the effective mass of the slab for the initial phase, by assuming the slab's deformed shape to be similar to that of a built-in section and using this as a shape function for the evaluation of the generalised mass:

$$\varphi(x) = 12 \left( \frac{x}{L_{eff}} \right)^2 - 16 \left( \frac{x}{L_{eff}} \right)^3 \tag{33}$$

The mass is then worked out using:

$$m_{s0} = 2\pi \rho_c h_s^2 \int_0^{2\pi} \int_0^{\frac{L_{eff}}{2}} [\varphi(x)]^2 \, dx \, d\theta \tag{34}$$

Substituting (33) into (34), then it can easily be shown that $m_{s0} \approx 2800 h_s^2 L_{eff}$ assuming $\rho_c = 2400$ kg/m$^3$, which is typical for normal weight concrete.

– Slab damping

The damping parameter, $c_{s0}$, is obtained using the standard expression from structural dynamics as:

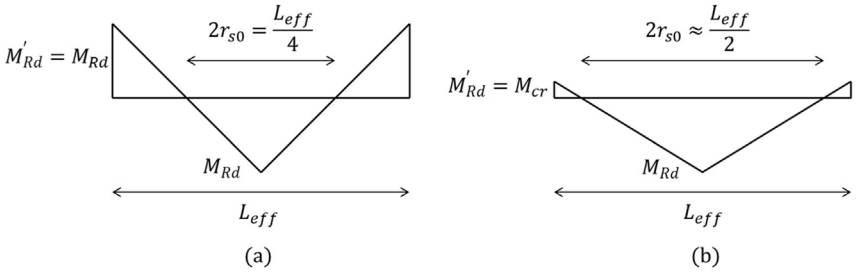


**Fig. 21.** Reduced slab span: (a) Equal top and bottom reinforcement; (b) No top reinforcement.

$$c_{s0} = 2\zeta m_{s0}\sqrt{\frac{k_{s0}}{m_{s0}}} \tag{35}$$

where $\zeta$ is the structure's damping co-efficient, which depends on the structural type.

Further discussion on the value of this parameter is done in Section 4.

– Contact stiffness

Finally, the contact stiffness, $k_c$, is set such that the impactor's and slab's displacement are equal at $t = t_c$ and by assuming the Hertz contact law given by:

$$F_c = k_c(u_i - u_s)^{3/2} \tag{36}$$

The value of contact stiffness is obtained by an iterative process until it has a value such that the above condition is satisfied.

– Governing equations of motion

Having established all the mass, spring and damping parameters, it is now possible to write the governing equations of motion for the first phase:

$$\begin{cases} m_i(\ddot{u}_i + g) + k_c(u_i - u_s)^{3/2} = 0 \\ m_{s0}\ddot{u}_s + c_{s0}\dot{u}_s + k_{s0}u_s - k_c(u_i - u_s)^{3/2} = 0 \end{cases} \tag{37}$$

The system of equations shown in (37) is solved by numerical means (e.g. fourth-order Runge–Kutta method), subject to the initial conditions $u_s = 0$ and $\dot{u}_i = \sqrt{2gh_i}$ at $t = 0$.

At the end of the contact phase, the slab displacement $u_s$ is obtained and this is used as an initial condition for the post-contact phase. In addition, the strain and kinetic energy in the slab are also evaluated from which the slab velocity is obtained.

*3.2.2. Post-contact phase*

In the post-contact phase, the slab is assumed to undergo free vibration subject to the initial conditions obtained at the end of the contact phase. The governing differential equation, as per Fig. 19(b), is simply given by:

$$m_s\ddot{u}_s + c_s\dot{u}_s + k_s u_s = 0 \tag{38}$$

The slab load-rotation relationship (hence $k_s$) is obtained using (31) and (32) but the slab radius $r_s$ now increases from $r_{s0}$ to the actual slab dimension. This increase is assumed to occur linearly over time at a velocity of $v_c$ given by (26). A word on the value of $G_c$ is in order here. The elastic value of $G_c$ is given from classical mechanics as:

$$G_c = \frac{E_c}{2(1+\nu)} \tag{39}$$

where $E_c$ is the concrete elastic modulus (varying from 30 to 40 GPa for typical $f_c$ values [1]) and $\nu$ is the Poisson's ratio (equal to 0.2 [1]). Thus, from (39), $G_c$ has values typically ranging from around 12–17 GPa.

As the concrete cracks, the modulus decreases and hence $G_c$ decreases by a factor $\beta$ which reduces from 1 to 0 depending on the crack width. This reduction of $G_c$ affects $v_c$, according to (26), which could delay or interrupt the transition from $r_{s0}$ to $r_s$. However, the effect on $v_c$ is not significant, with the wave speed still remaining over 1000 m/s even for low $G_c$ values, as shown in Fig. 22. This implies that in typical slab applications (where $r_s$ is expected not to exceed around 2 m), the transition time is unlikely to exceed a duration of the order of 2 ms.

Similarly, $m_s$ is determined using (34) with the shape function based on the static deformation of the slab. From (38), the slab response is determined and thus the full load-rotation response can be established.

The entire procedure is summarised in Appendix A.

*3.2.3. Strain-rate*

From the displacements obtained using the two phase model described, the slab rotations can easily be established by assuming that the slab has a conical form beyond the critical crack [51,52] and thus the rotation can be evaluated by considering the displacement at any point $x$ away from the critical shear crack.

Thus, the crack width, $w$, can be determined from the fundamental assumption of the CSCT:

$$w \propto \psi d \tag{40}$$

In this paper, it is assumed that the proportionality constant is given by 0.5, as suggested by Fernández Ruiz and Muttoni [53].

Thus, the strain at the crack (assuming the reinforcement is within the elastic domain) can be established by using a strain-crack width relationship, such as the square root model suggested by Fernández Ruiz et al. [61]:

$$\varepsilon = \left(\frac{3\tau_{b,max}\psi d}{2\phi\sqrt{E_s f_y}}\right)^{2/3} \tag{41}$$

where $\tau_{b,max}$ is the maximum bond stress given by $f_c^{2/3}$. The square root model for bond is based on the affinity hypothesis of the slip distribution along long anchored bars and neglects the local loss of bond stiffness and strength due to the formation of local diagonal cracks [61].

The strain-rate $\dot{\varepsilon}$ can be determined from (41) as:

$$\dot{\varepsilon} = \frac{d}{dt}(\varepsilon) = \left(\frac{3\tau_{b,max}d}{2\phi\sqrt{E_s f_y}}\right)^{2/3}\left(\dot{\psi}\right)^{2/3} \tag{42}$$

Knowing the strain-rate from (42), it is possible to evaluate the corresponding effect on the failure criterion, as discussed in Section 2.4, and also to adjust $f_c$ and $f_y$ while establishing the slab load-

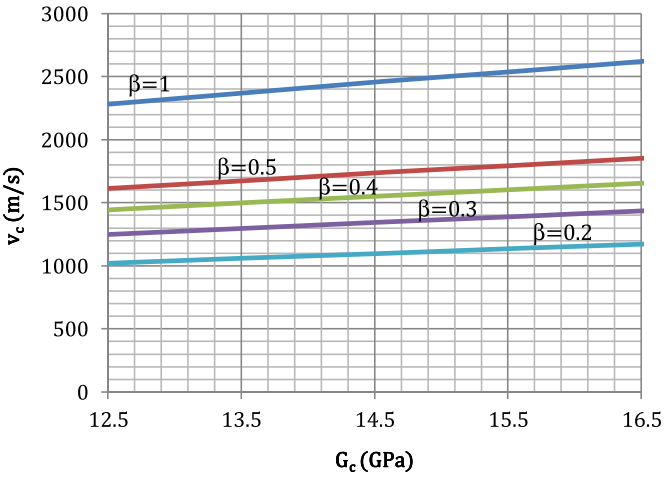


**Fig. 22.** Variation of $v_c$ with $G_c$.

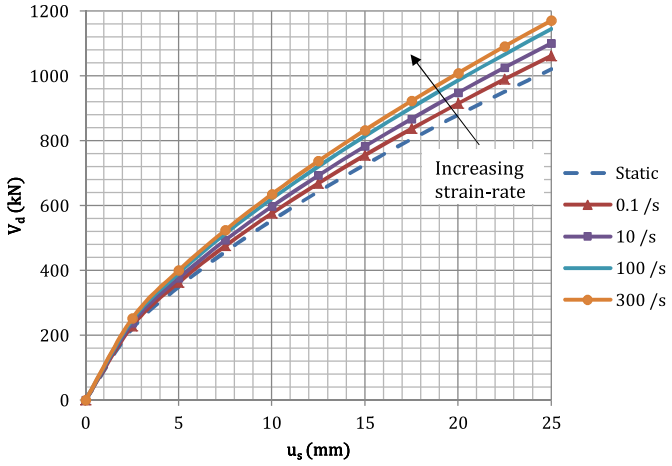


**Fig. 23.** Effect of increasing material properties due to strain-rate on slab stiffness.

rotation curve. However, the effects of strain-rate on the slab stiffness are found to be small (although not insignificant), as illustrated by Fig. 23 for a typical flat slab structure ($h_s = 280$ mm, $f_c = 30$ MPa, $\rho = 0.7\%$). For the case of $\dot{\varepsilon} = 0.1$/s. the increase in stiffness is by 4% while for $\dot{\varepsilon} = 300$/s, the increase is almost 15%.

At this point, a comment on alternative methods of estimating the strain-rate is in order. A simplified equation is presented in the American UFC 3-340-02 [62] to estimate the strain-rate in the concrete as:

$$\dot{\varepsilon} = \frac{0.002}{t_E} \tag{43}$$

where $t_E$ is the time duration from the initial impact to the peak response. The results obtained using (42) and (43) will be discussed and compared in Section 4.3.

## 4. Case studies

In this section, the use of the integral model proposed in this paper, as described in Sections 2 and 3, will be illustrated by assessing various impact loading scenarios on RC slabs.

### 4.1. Slabs with transverse reinforcement

In this section, the tests carried out by Delhomme et al. [28,45] will be investigated. Delhomme tested 12 × 4.8 × 0.28 m slabs reinforced top and bottom equally with $\rho = 0.71\%$ and having shear reinforcement $\rho_v = 0.36\%$. The concrete used had a compressive and tensile strengths of $f_c = 40.5$ MPa and $f_t = 5.8$ MPa respectively

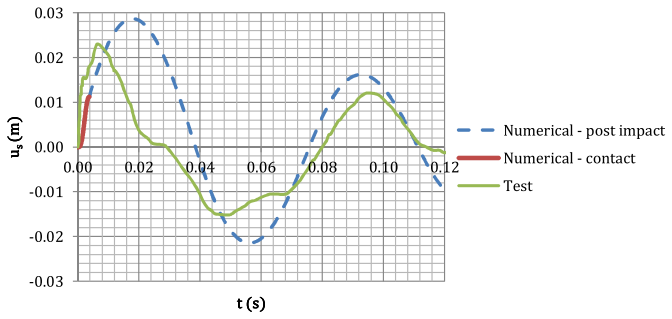


**Fig. 24.** Numerical and experimental displacement–time histories for T5.

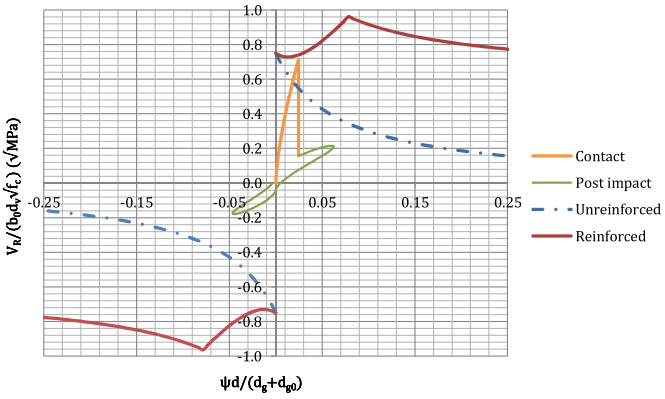


**Fig. 25.** Load-rotation response and failure criterion for T5.

whereas the yield strength of the flexural reinforcement was $f_s = 500$ MPa. The slabs were subjected to impact loadings from a 450 kg mass from a height of 30 m and 15 m (T5 and T1).

– Test T5

The displacement–time history was recorded and this was compared with the numerical result, as shown in Fig. 24.

Good correlation in terms of the maximum displacements and also temporally was observed, with the maximum predicted displacement being 28 mm and the maximum recorded displacement being 23 mm. The differences in the post-contact stage are expected as the analytical model neglects any bouncing effect between the impactor and the slab after impact (i.e. relative movement between the impactor and the slab is assumed to be zero).

As described in Section 3.1, the contact time and force were also accurately correlated.

From the displacements, the rotations were extracted and the load-rotation curve was assembled. The failure criterion from (5) was adjusted to take into account the strength contribution of the shear reinforcement, using the method proposed in Ref. [53]. Thus, the shear demand and strength are plotted together as shown in Fig. 25. In this instance, the strength and stiffness are based on the static values without any adjustment for strain-rate effects.

It can be observed that during contact, the stiffness is considerably higher than the post-contact phase.

In addition, both during loading and the free vibration phases, the maximum shear demand does not exceed the failure criterion, albeit that the slab is on the cusp of failure. Delhomme et al. record

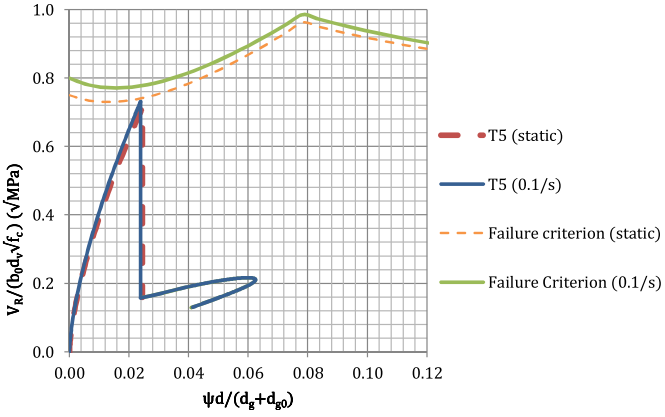


**Fig. 26.** Effect of strain-rate on load-rotation response and failure criterion for T5.

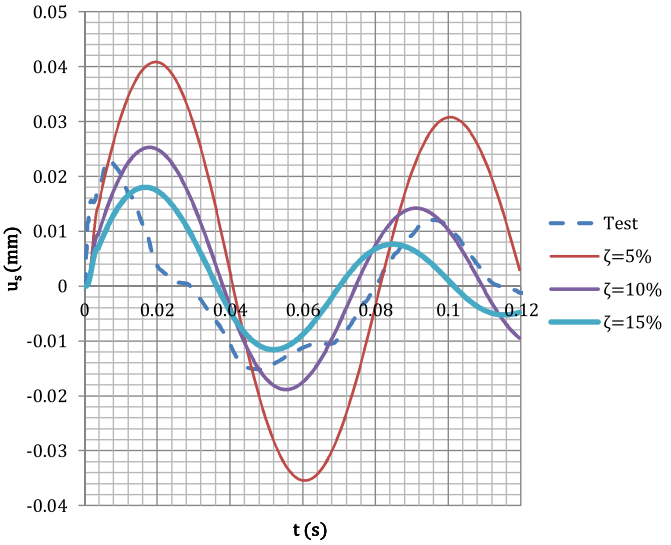


**Fig. 27.** Effect of Y parameter on displacement–time history for T5.

severe concrete cracking, indicating that concrete capacity is exceeded. However, complete punching was prevented by the shear reinforcement.

*4.1.1. Strain-rate effect*

As discussed in Section 2.4, strain-rate has a favourable effect on the failure criterion (thus the shear capacity) and also on the slab stiffness. In this case, using the procedure described in Section 3.2.3, the maximum strain-rate was estimated, using (42), to be 0.1/s for this case. These effects are illustrated in Fig. 26.

It can be observed that, in this case, there is little modification due to strain-rate effects to the load-rotation curve and the failure criterion and using the static curve for the latter will provide a conservative and accurate estimate of the slab's capacity.

*4.1.2. Damping ratio*

The only parameter which was not explicitly derived in the two phase model is the damping parameter ($c_{s0}$ and $c_s$), which depends on the choice of ζ. Fig. 27 shows the effect of the ζ on the response, suggesting that the correlation between the experimental and numerical results is best achieved with ζ = 10%. Indeed, Delhomme et al. measured ζ = 11%.

Whilst the selection of ζ remains a judicious choice to be done by the engineer, based on experience on similar structures, it is suggested that the value of ζ is taken between 5 and 10%.

– Test T1

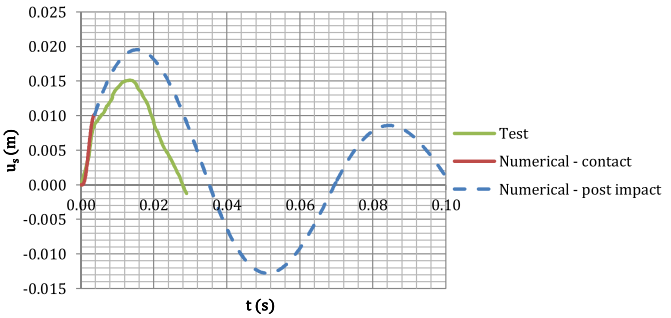


**Fig. 28.** Numerical and experimental displacement–time histories for T1.

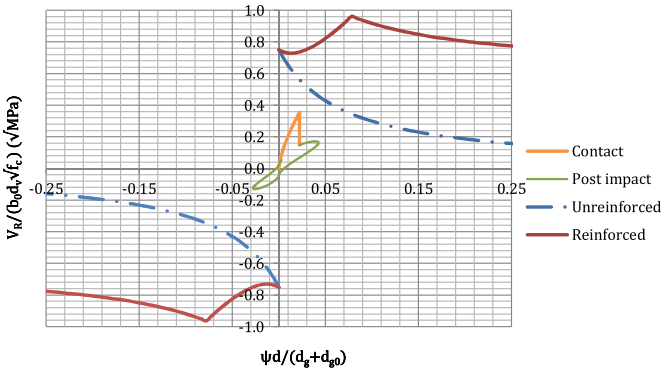


**Fig. 29.** Load-rotation response and failure criterion for T1.

A similar comparison between experimental results and numerical predictions was done in this case, with the correlation being as shown in Fig. 28.

The load-rotation and failure criterion are shown in Fig. 29. Since a strain-rate of around 0.08/s was predicted, the static values were used for the load-rotation curves, on the basis of the discussion earlier. Clearly, the maximum shear force is less than the capacity in this case.

Comparing Figs. 29 and 25, it can be observed that in the case of the higher drop height (T5), the stiffness is significantly higher, matching experimental observations. It can also be seen that the maximum rotation predicted is also higher in the case of the higher drop height (or larger contact force).

*4.2. Slabs with no transverse reinforcement*

In this section, the tests carried out by Bhatti et al. [36] will be investigated.

Bhatti tested 1.65 × 1.65 × 0.15 m slabs reinforced at the bottom with ρ = 0.6% and having no reinforcement at the top and also no transverse reinforcement. Only control slabs without FRP strips are considered in this work. The slabs were subjected to impact loadings from a 300 kg mass at 4 m/s and 5 m/s (N-IS-4 and N-IS-5). In both cases, punching shear failure was observed, as shown in Fig. 30.

– Test N-IS-4

The numerical prediction for this case is shown in Fig. 31. In this case, the maximum strain-rate was estimated using (42) to be 0.025/s and thus the static values were retained for both the stiffness and failure criterion.

The prediction is that the slab fails due to punching shear and this was confirmed by the test, as shown in Fig. 30(a).

– Test N-IS-5

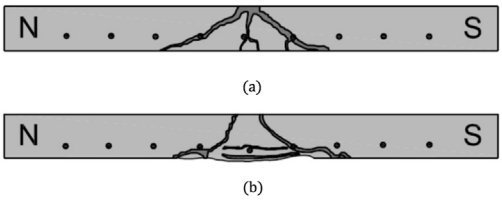


**Fig. 30.** Slab cross-sections showing punching failure: (a) N-IS-4; (b) N-IS-5 (after [36]).

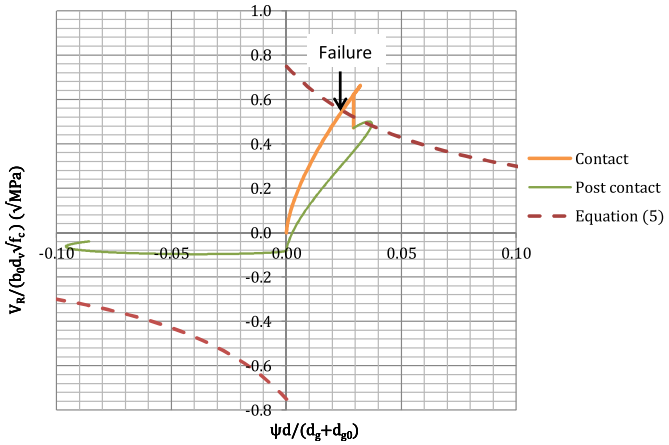


**Fig. 31.** Load-rotation response and failure criterion for N-IS-4.

The numerical prediction for this case is shown in Fig. 32. The maximum strain-rate was predicted to be around 0.035/s, from (42), and thus even in this case the static values were retained for both stiffness and strength. The model also predicts due to punching shear and this was also confirmed by the experimental test, as shown in Fig. 30(b).

Comparing the crack formation in the two specimens as shown in Fig. 30, it can be observed that in the case of the lower loading rate (N-IS-4), the flexural cracks leading to the shear cracks are wider than in the case of the higher loading rate (N-IS-5). This is also predicted by the model, which suggests that the normalised slab rotation (hence crack width) at failure is around 0.018 in the case of N-IS-5 and approximately 0.025 for N-IS-4.

This highlights the ability of the model to provide not only verification on whether the impacted slab has failed or not but also an indicative value of the slab deformation at failure. This is important data for the designer since in most codes of practice (e.g. UFC 3-340-02 [62]) use slab rotations to specify levels of acceptable damage in the design of RC structures subjected to extreme loading.

### 4.3. Strain-rate estimation

The strain-rates in the preceding sections were computed using the method proposed in this paper, i.e., using (42). In order to validate the suitability of the assumptions made in the derivation of (42) as discussed in Section 3.2.3, the estimated strain-rates are

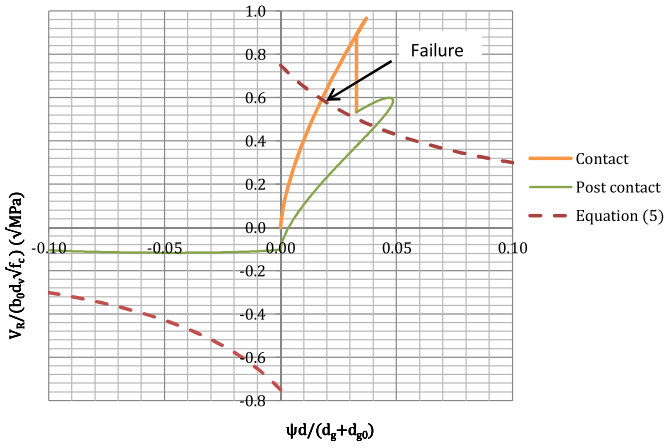


**Fig. 32.** Load-rotation response and failure criterion for N-IS-5.

**Table 3**
Comparison of strain-rate values.

| Test | $\dot{\varepsilon}$ (/s) | |
|---|---|---|
| | Proposed method eq'n (42) | UFC method eq'n (43) |
| T5 | 0.1 | 0.112 |
| T1 | 0.08 | 0.130 |
| N-IS-4 | 0.025 | 0.075 |
| N-IS-5 | 0.035 | 0.072 |

compared with values obtained using (43), which has been historically been used to estimate strain-rates since the 1990s (e.g. in TM 5-1300 [63]).

The comparison is shown in Table 3.

It can be observed that, in all cases, the two equations predict strain-rates within the same order of magnitude which, given that both stiffness and strength are only significantly affected by strain-rate when this changes by several orders of magnitude, then it can be concluded that the proposed method produces relatively accurate estimates of strain-rate values which complement the remainder of the model presented in this paper.

## 5. Concluding remarks

In this paper, a two-phase model which can predict the dynamic response of RC slabs subjected to impact loading has been presented. This model provides the shear demand on a structure, taking into account the effects of strain-rate on the material properties and also the initial increased stiffness of the structure due to inertial effects.

The slab stiffness and response is evaluated during the contact and post-contact phases and it is found that the increase in stiffness reported by other researchers is dominated primarily by the effective reduction in the slab's span rather than by enhancements to material properties due to strain-rate effects, except for very high strain-rates ($\dot{\varepsilon} \gtrsim 100$/s). The model is used to assess the behaviour of a slab subjected to a known impact scenario.

In addition, in this paper the failure criterion proposed in the latest version of the Model Code to predict punching shear failure in the static case has been extended to take into account the effects of strain-rate and thus provide a variation of the dynamic shear strength supply with slab deformation (rotation). It is found that punching shear strength is only markedly increased for strain-rates in excess of 100/s.

The model's governing equations are solved numerically and used for various slabs with and without transverse reinforcement which are subjected to localised impact loading. The model is used to predict the slab's behaviour and assess the occurrence of failure due to punching shear. The model also provides information about the level of deformation (i.e. slab rotation) at failure. The good correlation between experimental (from Refs. [28,36,46]) and predicted results suggests the plausibility of the proposed model.

The advantage of the proposed method is that, unlike previous methodologies, the current work follows an integral approach in which both the loading on the structure (shear demand) as well as its capacity (shear strength supply) are predicted.

## Acknowledgements

This work is part of a research project financially supported by the Engineering and Physical Sciences Research Council (E.P.S.R.C.) of the U.K. (grant reference: EP/K008153/1).

## Appendix A

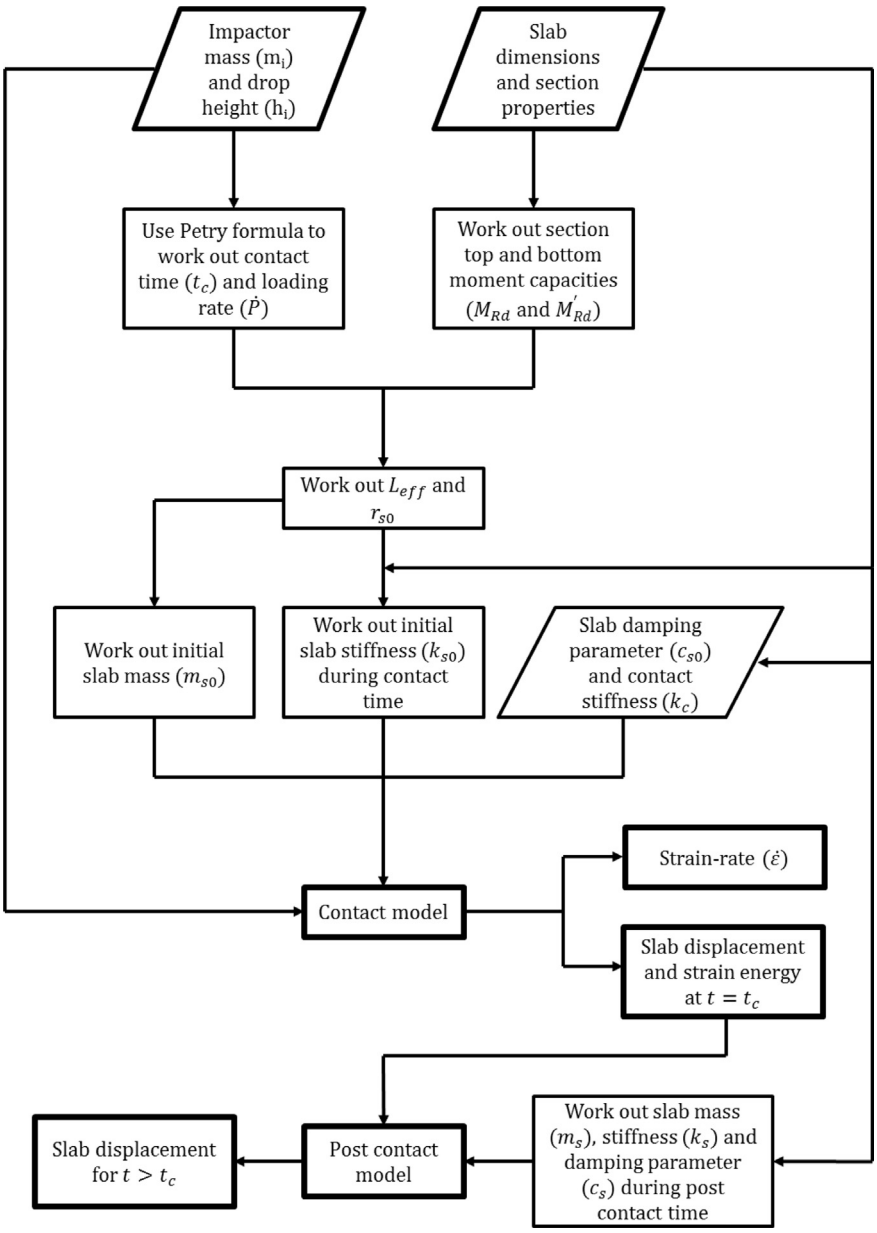


## References


[1] Bulletin 65: model code 2010 (volume 1) final draft. CEB/fib; 2010.
[2] Cormie D, Mays G, Smith P. Blast effects on buildings. 2nd ed. London: ICE Publishing; 2012.
[3] Yon J-H, Hawkins NM, Kobayashi AS. Strain-rate sensitivity of concrete mechanical properties. ACI Mater J 1992;89(2):146–53.
[4] Malvar LJ, Ross CA. Review of strain-rate effects for concrete in tension. ACI Mater J 1998;95(6):735–9.
[5] Lambert DE, Allen Ross C. Strain-rate effects on dynamic fracture and strength. Int J Impact Eng 2000;24(10):985–98.
[6] Grote DL, Park SW, Zhou M. Dynamic behaviour of concrete at high strain-rates and pressures: I. experimental characterisation. Int J Impact Eng 2001;25(9):869–86.
[7] Li QM, Meng H. About the dynamic strength enhancement of concrete-like materials in a split Hopkinson pressure bar test. Int J Solids Struct 2003;40(2):343–60.
[8] Schuler H, Mayrhofer C, Thoma K. Spall experiments for the measurement of the tensile strength and fracture energy of concrete at high strain-rates. Int J Impact Eng 2006;32(10):1635–50.
[9] Weerheijm J, Van Doormaal JCAM. Tensile failure of concrete at high loading rates: new test data on strength and fracture energy from instrumented spalling tests. Int J Impact Eng 2007;34(3):609–26.
[10] Yan D, Lin G, Chen G. Dynamic properties of plain concrete in triaxial stress state. ACI Mater J 2009;106(1):89–94.
[11] Lu YB, Li QM. About the dynamic uniaxial tensile strength of concrete-like materials. Int J Impact Eng 2011;38(4):171–80.
[12] Cotsovos DM, Pavlovi&cacute MN. Numerical investigation of concrete subjected to high rates of uniaxial tensile loading. Int J Impact Eng 2008;35(5):319–35.
[13] Bull 66: model code 2010 (volume 2) final draft. CEB/fib; 2010.
[14] Model code 1990. CEB/fib; 1993.
[15] Mindess S, Banthia N, Yan C. The fracture toughness of concrete under impact loading. Cem Concr Res 1987;17:231–41.

[16] Brara A, Klepaczko JR. Fracture energy of concrete at high loading rates in tension. Int J Impact Eng 2007;34(3):424–35.
[17] Zhang XX, et al. Fracture behaviour of high-strength concrete at a wide range of loading rates. Int J Impact Eng 2009;36(10–11):1204–9.
[18] Oh BH. Fracture behaviour of concrete under high-rates of loading. Eng Fract Mech 1990;35:327–32.
[19] Campbell JD. The dynamic yielding of mild steel. Acta Metall 1953;1(6):706–10.
[20] Mainstone RJ. Properties of materials at high rates of straining or loading. Mater Struct 1975;8(2):102–16.
[21] Johnson GR, Cook W. Fracture characteristics of three metals subjected to various strains, strain rates, temperatures and pressures. Eng Fract Mech 1985;21(1):31–48.
[22] Cowper GR, Symonds PS. Strain-hardening and strain-rate effects in the impact loading of cantilever beams. Brown University (Dept. of Appl. Math.); 1957.
[23] Hughes G, Beeby AW. Investigation of the effect of impact loading on concrete beams. Struct Eng 1982;60B(3):45–52.
[24] Ross TJ, Krawinkler H. Impulsive direct shear failure in RC slabs. ASCE J Struct Eng 1985;111(8):1661–77.
[25] Miyamoto A, King MW, Fujii M. Analysis of failure modes for RC slabs under impulsive loads. ACI Struct J 1991;88(5):538–45.
[26] Miyamoto A, King MW, Fujii M. Nonlinear dynamic analysis of RC slabs under impulsive loads. ACI Struct J 1991;88(4):411–9.
[27] Saito H, et al. Loading capacities and failure modes of various reinforced-concrete slabs subjected to high speed loading. Nucl Eng Des 1995;156(1–2):277–86.
[28] Delhomme F, et al. Simulation of a block impacting a reinforced concrete slab with a finite element model and a mass-spring system. Eng Struct 2007;29(11):2844–52.
[29] Zineddin M, Krauthammer T. Dynamic response and behaviour of reinforced concrete slabs under impact loading. Int J Impact Eng 2007;34(9):1517–34.
[30] Cotsovos D, Stathopoulos N, Zeris C. Behaviour of RC beams subjected to high rates of concentrated loading. ASCE J Struct Eng 2008;134(12):1839–51.
[31] Chen Y, May IM. Reinforced concrete members under drop-weight impacts. Proc ICE – Struct Build 2009;162(1):45–56.
[32] Izatt C, et al. Perforation owing to impacts on RC slabs. Proc ICE – Struct Build 2009;162(1):37–44.
[33] Saatci S, Vecchio FJ. Effects of shear mechanisms on impact behaviour of reinforced concrete beams. ACI Struct J 2009;106(1):78–86.
[34] Abbas AA, Pullen AD, Cotsovos D. Structural response of RC wide beams under low-rate and impact loading. Mag Concr Res 2010;62(10):723–40.
[35] Cotsovos DM. A simplified approach for assessing the load-carrying capacity of reinforced concrete beams under concentrated load applied at high rates. Int J Impact Eng 2010;37(8):907–17.
[36] Bhatti AQ, Kishi N, Tan KH. Impact resistant behaviour of RC slab strengthened with FRP strips. Mater Struct; 2011.
[37] Ožbolt J, Sharma A. Numerical simulation of reinforced concrete beams with different shear reinforcements under dynamic impact loads. Int J Impact Eng 2011;38(12):940–50.
[38] Jiang H, Wang X, He S. Numerical simulation of impact tests on reinforced concrete beams. Mater Des 2012;39(0):111–20.
[39] Mokhatar SN, Abdullah R. Computational analysis of reinforced concrete slabs subjected to impact loads. Int J Integr Eng 2012;4(2):70–6.
[40] Magnusson J, Hallgren M, Ansell A. Air-blast-loaded, high-strength concrete beams. Part I: experimental investigation. Mag Concr Res 2010;62(2):127–36.
[41] Magnusson J, Ansell A, Hansson H. Air-blast-loaded, high-strength concrete beams. Part II: numerical non-linear analysis. Mag Concr Res 2010;62(4):235–42.
[42] Abdel-Rohman M, Sawan J. Impact effect on RC slabs – analytical approach. ASCE J Struct Eng 1985;111(7):1590–601.
[43] Sawan J, Abdel-Rohman M. Impact effect on RC slabs – experimental approach. ASCE J Struct Eng 1986;112(9):2057–65.
[44] CEB. Bulletin 187: concrete structures under impact and impulsive loading. CEB; 1988.
[45] Delhomme F. Étude du comportement sous impact d'une structure pareblocs en béton armé. Universite de Savoie; 2005.
[46] Barbier F, Roby M. Simplified unified model for concrete structures under impact. In: Fib symposium 2013; 2013. Israel.
[47] ACI. ACI 318-08-building code requirements for structural concrete; 2008. Michigan (USA).
[48] BSI. BS 8110-1-structural use of concrete. Code of practice for design and construction; 1997. London (UK).
[49] CEN. EN 1992-1-1-design of concrete structures – part 1-1: general rules and rules for buildings; 2004. Brussels (Belgium).
[50] Muttoni A. SIA draft code proposal (SIA 162/AG5). Zürich, Switzerland: Swiss Federal Institute of Technology; 1988.
[51] Muttoni A. Punching shear strength of reinforced concrete slabs without transverse reinforcement. ACI Struct J 2008;105(4):440–50.
[52] Muttoni A, Ruiz MF. Shear strength of members without transverse reinforcement as function of critical shear crack width. ACI Struct J 2008;105(2):163–72.
[53] Ruiz MF, Muttoni A. Applications of critical shear crack theory to punching of reinforced concrete slabs with transverse reinforcement. ACI Struct J 2009;106(4):485–94.
[54] Sagaseta J, et al. Non-axis-symmetrical punching shear around internal columns of RC slabs without transverse reinforcement. Mag Concr Res 2011;63(6):441–57.
[55] Hillerborg A, Modéer M, Petersson PE. Analysis of crack formation and crack growth in concrete by means of fracture mechanics and finite elements. Cem Concr Res 1976;6(6):773–81.
[56] Hordijk DA. Local approach to fatigue of concrete. Delft: Delft University of Technology; 1991.
[57] Guidotti R. Poinçonnement des planchers-dalles avec colonnes superposées fortement sollicitées. Lausanne: École Polytechnique Fédérale de Lausanne; 2010.
[58] Walraven JC. Aggregate interlock: a theoretical and experimental analysis. Delft: Delft University of Technology; 1980.
[59] Lui LM. Shear strength of concrete joints under dynamic loads. Hong Kong: University of Hong Kong; 1977.
[60] Muttoni A, Ruiz MF. The levels-of-approximation approach in MC 2010: application to punching shear provisions. Struct Concr 2012;13(1):32–41.
[61] Ruiz MF, Muttoni A, Gambarova PG. Analytical modeling of the pre- and postyield behaviour of bond in reinforced concrete. ASCE J Struct Eng 2007;133(10):1364–72.
[62] UFC 3-340-02-structures to resist the effects of accidental explosions. USA Department of Defense; 2008.
[63] TM 5-1300-structures to resist the effects of accidental explosions. Department of the Army; 1990.